Journal of Materials Chemistry A

PAPER

View Article Online
View Journal | View Issue

Cite this: J. Mater. Chem. A, 2015, 3, 21321

An electrochromic supercapacitor and its hybrid derivatives: quantifiably determining their electrical energy storage by an optical measurement†

Minshen Zhu,[a] Yang Huang,[a] Yan Huang,[a] Wenjun Meng,[a] Qingchao Gong,[b] Guangming Li[b] and Chunyi Zhi*[ac]

Received 9th August 2015
Accepted 11th September 2015

DOI: 10.1039/c5ta06237c

www.rsc.org/MaterialsA

In this article, an electrochromic supercapacitor was developed with the electrode material active for both electrochromism and energy storage. The detailed measurements of the optical spectra of the device revealed that the normalized optical density, a concept in electrochromic studies, depended linearly on the electrical energy storage (EES) of the supercapacitor. This enabled the precisely quantifiable determination of a solid-state supercapacitor's EES by simple optical transmission measurement, which is demonstrated here for the first time, to the best of our knowledge. One step further, parallel-structured hybrid supercapacitors were designed to integrate the developed smart function with high-performance supercapacitors using polypyrrole (PPy) and manganese oxide (MnO_2) as electrode materials. The developed hybrid supercapacitors exhibited excellent capacitive performance and maintained the ability of electrochromic EES indicators well. Different calibration curves can be produced for different types of hybrid supercapacitors. With these curves, the EES of hybrid supercapacitors can be precisely determined using a simple optical transmission measurement. Our study paves the way for the integration of electrochromic EES indicators in various energy storage devices, as well as the prompt and quantitative determination of the EES of various types of supercapacitors using a simple optical transmission measurement.

1. Introduction

The development of efficient energy storage devices has attracted a lot of attention because of the urgent requirements for utilizing renewable energy as a substitute for traditional energy.[1–4] Among the strategies of effectively storing energy, electrochemical capacitors, also named supercapacitors, are a kind of promising device for energy storage due to their long cycle life, superior power density and good rate ability.[3–6] Beside a strong focus on improving the electrochemical performance of supercapacitors,[7–13] integration with multi-functions, such as flexibility and wearable compatibility,[14–23] has increasingly attracted the interest of researchers for convenient usage of supercapacitors in portable devices. In addition, incorporating some smart functionalities in supercapacitors for easy use in daily life is another important issue for developing supercapacitors.[24–26] Among these issues, it is important to allow people to easily and in real time estimate or determine the storage of electrical energy. Therefore, using or incorporating smart materials that can be used for easily determining the electrical energy storage is of great significance.[27–32]

For an easy estimation of energy storing states, variation of the active materials should be easily sensed by humans. The visual change is the most impressive change to be identified. Meanwhile, some transition-metal oxides or conductive polymers (*e.g.* polyaniline) can serve as active materials for both supercapacitors and electrochromic devices because they all utilize fast faradaic reactions between the active materials and electrolytes.[33–36] Therefore, these kinds of materials are suitable for the fabrication of smart supercapacitors. Among these materials, tungsten oxides have been reported to have been used as smart materials for supercapacitors due to their great compatibility for both supercapacitors and electrochromic devices, as well as the perfect contrast between the bleached state (transparent) and colored state (dark blue). The smart function has been successfully demonstrated by relating the change in color to the potential or electrical energy storage (EES) of the working electrode.[27–33]

[a]Department of Physics and Materials Science, City University of Hong Kong, 83 Tat Chee Avenue, Kowloon, Hong Kong, P. R. China. E-mail: cy.zhi@cityu.edu.hk

[b]School of Mechanical, Electrical & Information Engineering, Shandong University, Weihai, P. R. China

[c]Shenzhen Research Institute, City University of Hong Kong, Shenzhen, 518057, P. R. China

† Electronic supplementary information (ESI) available: XRD patterns of e-WO_3, the table of the electrical energy storage (EES) obtained from the idea and tested galvanostatic curves, the transmission spectrum when EES is 0%, and the cyclic voltammetric and galvanostatic curves of e-WO_3//PPy and e-WO_3//MnO_2. See DOI: 10.1039/c5ta06237c

In spite of these demonstrations, at least three problems should be resolved to achieve an impeccable smart function. First of all, the color change can only be used for estimation, while how to quantitatively define color change and thus determine the associated supercapacitors' parameters remains a challenge. Secondly, only very few materials that are active for both electrochromic and electrochemical capacitors can be used as electrodes for this kind of smart device. As a result, the reported color-change smart supercapacitors usually possess limited capacitance,[29,31] while the smart function has not been realized for the high performance supercapacitors fabricated from excellent active materials, such as PPy and MnO_2.[37–40] Therefore, it is of great importance to develop a practicable approach to integrate smart functions and highly capacitive performance.

The third problem is a crucial and essential one: it is actually not clear whether the color change is associated with the potential or EES of the supercapacitors. It should be noted that the dependence between the potential and EES is not linear. This is because the galvanostatic curves tested for almost all types of supercapacitor electrodes, especially the pseudo ones, always present a serious distortion from an ideal triangle, as displayed in Fig. 1a, a typical galvanostatic curve for a WO_3 electrode. Therefore, a great deviation may be generated when calculating the EES from the potential by the popularly used equation

$$\mathrm{EES} = (E_{\mathrm{EES}} - E_0)/\Delta E,$$

where E_{EES} is the potential at a certain EES, E_0 is the potential at the initial state, and ΔE is the potential window. As shown in Fig. 1b, the intersection points of the grid intersection represent the calculated EES based on the assumption that the potential is linearly related to time, and they are emphasized by magenta dots. The blue circle and red diamond dots represent the actual EES calculated from the real charging and discharging curves, respectively. It is revealed that the deviation can be as large as 16.27% (Table S1 in the ESI†). Therefore, it becomes very important to clearly figure out if the color change is actually associated with the potential or EES of a supercapacitor, or to clarify how to associate the color change to the EES, as it is usually considered as an essential parameter for a supercapacitor as an energy storage device.

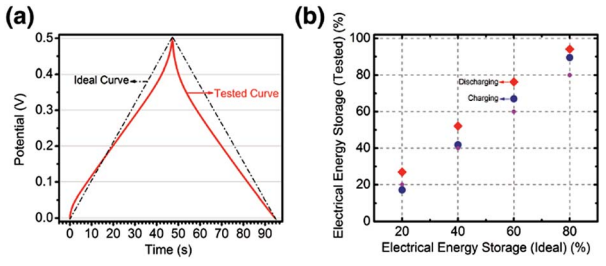

Fig. 1 Using potentials to estimate the EES of a supercapacitor through a simple equation may result in serious deviation due to the nonlinear dependence between them. (a) The deviation from an ideal triangular galvanostatic curve of the tested curve of an e-WO_3 electrode, and (b) the deviation of the EESs calculated from the ideal curve from those calculated by the tested curve. The charged and discharged EESs are represented by the red diamond dots and blue circle dots, respectively. The ideal EESs are indicated by the intersections of the grids, and they are highlighted by the magenta circle dots.

To solve the three problems mentioned above, herein, tungsten oxide (WO_3) was synthesized by a very facile electrodepositing method as the smart electrode material. Optical density, a concept in electrochromism studies, was introduced for a comprehensive investigation on the color change of the WO_3 film based supercapacitors. Then, a linear dependence between the normalized optical density and EES of the supercapacitor was discovered, which enables a precisely quantitative determination of the EES of the supercapacitor.

Subsequently, hybrid supercapacitors were successfully designed and fabricated in order to integrate the smart function of color-change based EES indicators to various high-performance supercapacitors. The calibration curves were developed for different hybrid supercapacitors, which makes it easy to quantitatively determine the EES of high-performance supercapacitors precisely using a simple optical transmission test.

2. Experimental

2.1. Fabrication of the e-WO_3 based solid-state supercapacitors

WO_3 was electrodeposited on the surface of FTO coated glass. The aqueous solution for the electrodeposition was prepared by the following process: Na_2WO_4 (1.65 g) was dissolved in deionized water (200 mL) followed by the addition of H_2O_2 (0.6 mL) under stirring. Subsequently, the pH of the electrolyte was adjusted to be 1.5 by adding HNO_3 (3 M). Afterwards, the electrodeposition process was carried out under constant voltage (−0.65 V *vs.* SCE) and lasted 300 s for balance between the transparency of the electrode and the capacitance. The weight was around 1 mg. The electrolyte for the solid-state supercapacitors was prepared by the following process: H_2SO_4 (6 g) was mixed with deionized water (60 mL) followed by the addition of PVA (6 g, molecular weight: ~100 000). Subsequently, the mixture was heated to 85 °C under stirring. When the mixture became transparent, the prepared electrodes were immersed into the hot electrolyte for several seconds. After the electrolyte solidified, the two electrodes were assembled.

2.2. Fabrication of the hybrid solid-state supercapacitors

For the e-WO_3//PPy hybrid electrodes, e-WO_3 was electrodeposited onto one zone of the FTO coated glass. Then, PPy was electrochemically polymerized under a constant voltage of 0.8 V referenced to saturated calomel electrode (SCE) onto the other zone of the FTO coated glass using an aqueous solution containing *p*-toluenesulfonic acid (0.1 M), sodium *p*-toluenesulfonic (0.3 M), and the pyrrole monomer (300 μL) for 90 s. The weight of PPy formed on the FTO was around 0.5 mg. The assembly process was similar to that of e-WO_3 based solid-state supercapacitors. For the fabrication of e-WO_3//MnO_2 hybrid supercapacitors, MnO_2 was electrodeposited using an electrolyte containing $Mn(NO_3)_2$ (20 mM) and $NaNO_3$ (100 mM) under

a constant current density of 0.5 mA cm^{-2}. The weight of MnO_2 formed on the FTO was around 0.5 mg. The assembly process was identical to that of e-WO_3//PPy hybrid solid-state supercapacitors.

2.3. Electrochemical tests and material characterizations

Electrochemical measurements were carried out on an electrochemical workstation (CHI660C). The crystallographic characteristics of the samples were investigated through X-ray powder diffraction using a BRUKER D2 PHASER diffractometer, which was equipped with Cu Kα irradiation (λ = 1.54184 Å) and working at 10 mA and 30 kV. The morphologies were investigated using an environmental scanning electron microscope (ESEM, FEI/Philips XL30), and a field emission transmission electron microscope (JEOL-2001F). UV-vis experiments were conducted in transmission mode with a UV-vis spectrophotometer (HALO DB20) over a wavelength range of 400–800 nm.

3. Results and discussion

3.1. Electrochromic supercapacitor and its EESs

Fig. 2a shows the scanning electron microscopy (SEM) images of the cross-section of the electrode based on e-WO_3. The thickness of the e-WO_3 film is about 970 nm, which not only enables sufficient coloring efficiency but also maintains the transparency of the electrode in the bleached state. It consists of nanoclusters of the e-WO_3 nanoparticles, which is shown in the inset in Fig. 2a. The transmission electron microscopy (TEM) image in Fig. 2b confirms the particle structures of the e-WO_3 film. Fig. 2c shows the high resolution transmission electron microscopy (HRTEM) image of e-WO_3, which reveals a structure embedding many small crystal nanoparticles in an amorphous matrix. This observed structure is consistent with the XRD patterns shown in Fig. S1 in the ESI† which shows a broad peak combined with several sharp peaks, corresponding to the amorphous and crystallized components of the e-WO_3 nanoparticle clusters. The crystal structure identified from the XRD patterns shows that e-WO_3 has a cubic phase (JCPDS no. 41-0905, cubic, *Pm*/3*m*). The amorphous matrix will benefit the electrochromic process due to its good stability and high contrast between the bleached and colored states.[42,43] The scheme in Fig. 2d shows the process of fabricating electrodeposited tungsten oxide (e-WO_3) based solid state supercapacitors. Briefly, e-WO_3 was electrodeposited onto the two FTO coated glasses, followed by the coating of the electrolyte (PVA–H_2SO_4). After the solidification of the electrolyte, the as-prepared two pieces of FTO coated glass were assembled together and intersected for the easy observation of the color variation at different EESs.

To reveal the electrochemical properties, the e-WO_3 film was first investigated in liquid electrolyte (0.5 M H_2SO_4) in the potential range from −0.5 V to 0 V referenced to the saturated calomel electrode (SCE). Fig. 3a and b show the cyclic voltammetric (CV) and galvanostatic curves. In addition to the near rectangular and symmetric shape of the CV curves measured at low scan rates of 5–20 mV s^{-1}, the anodic and cathodic peaks of e-WO_3 can also be clearly identified. These are typical features for pseudocapacitors, indicating that redox reactions are involved while great reversibility is kept. The obvious distortion of the CV curves can be found at high scanning rates (>50 mV s^{-1}), and results from the limited conductivity and time constant of the e-WO_3 film.[34] The galvanostatic curves (Fig. 3b) show the distortion from the ideal triangle with near symmetric shapes, which also represents a pseudocapacitive process. The area capacitance, which is believed to be more

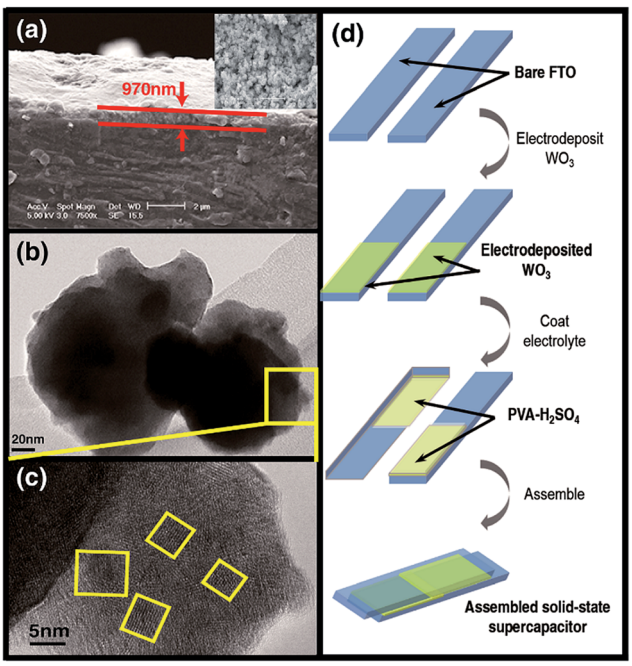

Fig. 2 (a) Cross-section SEM image of the e-WO_3 film, and the (b) TEM and (c) HRTEM images of the e-WO_3 nanoparticles. (d) Schematic of the process for the fabrication of the e-WO_3 solid-state supercapacitors.

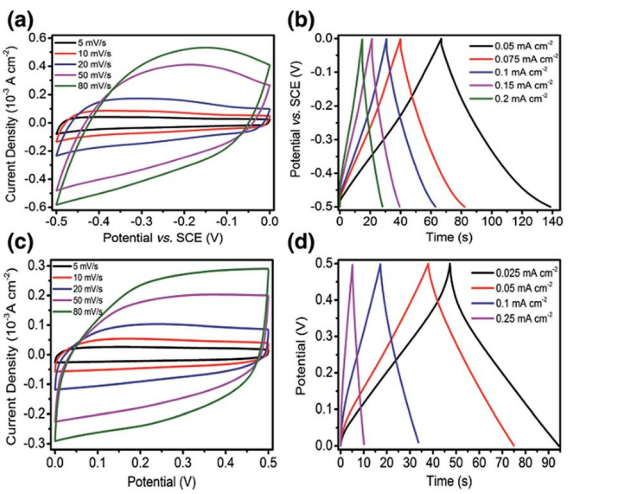

Fig. 3 (a) CV and (b) galvanostatic curves of e-WO_3 in 0.5 M H_2SO_4 electrolyte, and (c) CV and (d) galvanostatic curves of e-WO_3 in the solid-state supercapacitors.

reliable and practical, especially when the weight of active materials is very small, is accordingly used here.[41] And the area capacitance calculated from the galvanostatic curve reaches 10 mF cm^{-2} at the charging and discharging current of 0.05 mA cm^{-2}, showing the decent capability of e-WO_3 as an active material for supercapacitors. Fig. 3c and d show the typical CV and galvanostatic curves for the all solid-state supercapacitors with e-WO_3 electrodes. Typical pseudocapacitive behaviors are kept and the area capacitance of the e-WO_3 based solid-state supercapacitors reaches 3.5 mF cm^{-2} for the device and 7.0 mF cm^{-2} for the single electrode at a charging and discharging current of 0.05 mA cm^{-2}. This performance is comparable to that of other electrochromic supercapacitors based on WO_3, as can been seen in Table S2.† The decrease in the capacitance of the solid-state device is the result of the increase in bulk resistance and a more sluggish capacitive behavior due to the relatively poor contact between e-WO_3 and the solid-state electrolyte, which can be seen from the Nyquist plots in Fig. S2.†

For further confirmation of the capability of e-WO_3 serving as an active material for electrochromic supercapacitors, we took the SEM images of e-WO_3 after electrochromic and electrochemical processes (Fig. S3†). As no significant differences can be seen from Fig. S3,† the as-prepared e-WO_3 is suitable for being an active material for electrochromic supercapacitors.

Accompanying the energy storage following the reaction: $WO_3 + xH^+ + xe^- \rightarrow H_xWO_3$, the electrode will change from transparent to dark blue due to the increasing formation of blue color center W^{5+} polarons.[44–46] Photos in Fig. 4a show the color of the electrodes at different EESs, which certifies the color change as expected. The electrode at the pristine state (EES = 0%) is almost transparent. During the charging process, the color becomes darker and darker with the EES increasing from 0% to 100%. A fully charged (EES = 100%) supercapacitor exhibits a dark blue appearance due to the heavy formation of W^{5+}. Therefore, the EES can be easily estimated by identifying the color of the electrodes.

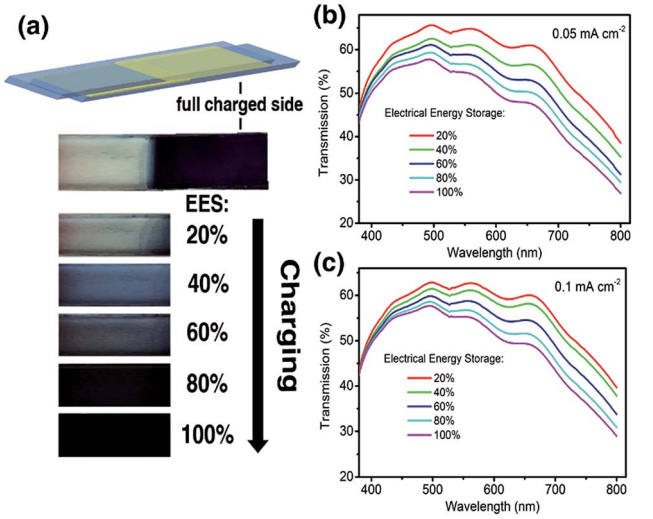

Fig. 4 (a) Photographs of the e-WO_3 electrode at different EESs, and the transmission spectra of the e-WO_3 electrode charged at different currents: (b) 0.1 mA, and (c) 0.2 mA.

The next target is to quantitatively determine the EES of the supercapacitor using the color change. Transmission spectra of the electrode were measured at a wavelength range of 400 to 800 nm under a charging/discharging current of 0.05 mA cm^{-2} and 0.1 mA cm^{-2}, respectively. It was revealed that the transmission continuously decreased during the charging process for both charging current densities. However, a detailed comparison indicates that the variation in the red light region (620–750 nm) is much more remarkable than that in the blue light region (450–475 nm). For example, with the supercapacitor being charged at 0.05 mA cm^{-2} to 100% EES (Fig. 4b), the transmission at the wavelength of 625 nm decreases by around 29%, while it decreases by 9% for the wavelength of 450 nm. Greater loss of red light transmission finally results in the dark blue color of the electrodes at high EES, which is in accordance with the photos shown in Fig. 4a. Therefore, the transmission in the red light region (for example, at the wavelength of 625 nm) can be an excellent indicator for the EES of the e-WO_3 based solid-state-supercapacitor.

Here, we introduce a concept popularly used in electrochromic studies, optical density, for further quantitative analyses.[30,32,33,42–47] The optical density is defined as $\log(T_{bleached}/T_{colored})$, where $T_{bleached}$ is the transmission in the bleached state, and $T_{colored}$ is related to the different transmissions during the electrochromic process. Furthermore, it is well known that the relationship between the optical density and the charge consumed during the electrochromic process (Q_c) can be expressed as:

$$\log(T_{bleached}/T_{colored}) = \eta \times Q_c \quad (1)$$

Here, η means the coloring efficiency of the as-prepared material, and is a constant because it is related to the nature of the as-prepared material.[30,32,33,42–47] Since the electrochromic process also means the charging process for the electrochromic supercapacitors, we can regard $T_{bleached}$ as the transmission at 0% EES (T_0), and $T_{colored}$ as the transmission at different EESs (T_{EES}). Moreover, Q_c can be expressed as $Q_c = EES \times Q_t$, where Q_t is the total charge that can be stored in the electrochromic supercapacitors in a certain situation. Therefore, the color change at different EESs can be quantifiably expressed using the equation:

$$\log(T_0/T_{EES}) = \eta \times EES \times Q_t \quad (2)$$

Since the value of Q_t may be different at different charging and discharging rates, the optical density is normalized by Q_t at certain charging and discharging rates. And the normalized optical densities at 625 nm *versus* the corresponding EESs are plotted in Fig. 5a and b. Accordingly, a linear dependence is clearly revealed. The fitted curve using $y = Ax + B$ is plotted as a dashed line in Fig. 5a and b. The fitted correlations (R) at different charging/discharging currents are both very close to 1 (0.99 for both 0.05 mA cm^{-2} and 0.1 mA cm^{-2}), which indicates a perfect linear dependence in spite of the charging/discharging

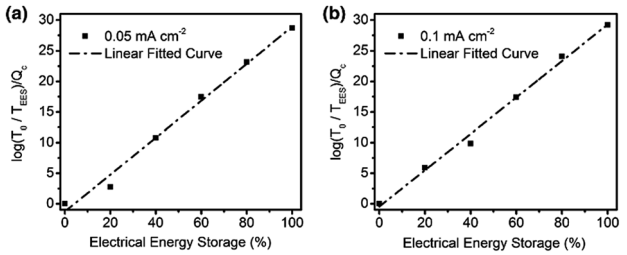

Fig. 5 Optical densities at 625 nm *versus* EES at charging/discharging currents of 0.1 mA (a) and 0.2 mA (b), respectively. A linear dependence is clearly revealed.

currents. By using these fitted curves, we can use the normalized optical density to reveal the EES of the supercapacitors. Furthermore, the difference between the values calculated from these two curves is less than 2%, as shown in Table S3 in the ESI,† which indicates the perfect accuracy. The introduction of optical density and its linear dependence on EES opens a way to quantitatively and precisely determine the EESs of a supercapacitor with simple optical transmission measurements using a spectrophotometer.

Back to the three problems mentioned in the introduction part, here we clarify that the color change is more related to the EES of a supercapacitor than to the potential. In addition, the optical density can be used to quantify the color change of the electrodes and it linearly depends on the EES of a supercapacitor with WO_3 as electrodes, and can serve as the indicator of EES for electrochromic supercapacitors.

3.2. Hybrid supercapacitors with an electrochromic EES indicator

To extend the applications of the developed smart supercapacitor and to solve the problem of the limited capacitance of the e-WO_3 electrodes, we developed and investigated hybrid solid-state supercapacitors that integrate the smart function of e-WO_3 to various high-performance supercapacitors. For universality purposes, we chose the two most popular supercapacitor materials, PPy and MnO_2, as the electrochemically active materials to investigate the relationship between the coloring process of the e-WO_3 part and the charging process of the whole device. The fabrication process is schematically shown in Fig. 6a. Briefly, WO_3 was deposited on one zone of the FTO coated glass, followed by PPy or MnO_2 being electrodeposited on the other zone. A copper wire is bridged between the two zones to form a parallel connection structure (Fig. 6b). Afterwards, coating the electrolyte and assembling the two pieces of electrode were done to form a hybrid solid-state supercapacitor. It is expected that with this parallel structure (Fig. 6b), the hybrid solid-state supercapacitors may take advantages of both the smart function of e-WO_3 and high capacitance from the highly capacitive active materials.

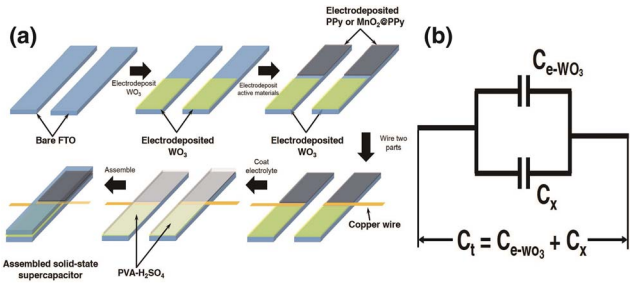

Fig. 6 (a) Schematic illustration of the fabrication process of the e-WO_3 based hybrid solid-state supercapacitors, and (b) the equivalent circuit for the fabricated hybrid supercapacitors.

The electrochemical performance of the as-prepared hybrid supercapacitors was investigated using CV and galvanostatic tests. Fig. 7a and S4† show the CV curves of the hybrid supercapacitors from e-WO_3 incorporated with the electrodeposited PPy (e-WO_3//PPy) and MnO_2 (e-WO_3//MnO_2). All curves measured at 20 mV s^{-1} in Fig. 7a exhibit typical pseudocapacitive behaviors. The distortion of the CV curve of e-WO_3//MnO_2 is severer than others due to the involved redox reactions and relatively low conductivity of MnO_2. The greatly improved

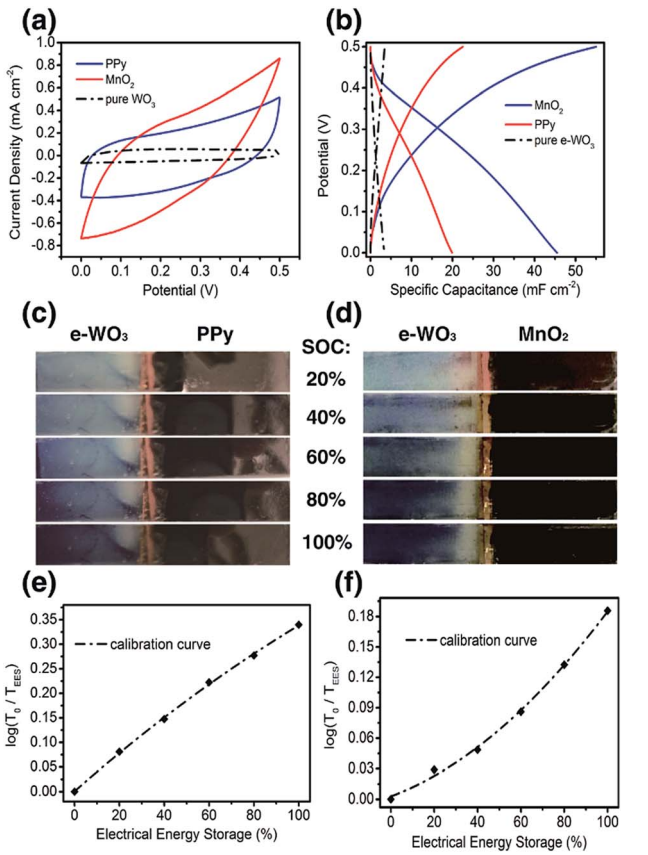

Fig. 7 (a) CV curves of the e-WO_3//PPy and e-WO_3//MnO_2 based hybrid supercapacitors at 20 mV s^{-1}; (b) galvanostatic charging/discharging curves of the e-WO_3//PPy and e-WO_3//MnO_2 based hybrid supercapacitors measured at a current density of 1 mA cm^{-2}; photos of the electrodes of the e-WO_3//PPy hybrid supercapacitors at different EESs (c) and e-WO_3//MnO_2 hybrid supercapacitors at different EESs (d) and the optical densities at 625 nm *versus* EES of the e-WO_3//PPy hybrid supercapacitors (e) and the e-WO_3//MnO_2 hybrid supercapacitors (f), which can be considered as a unique calibration curve solely produced for each type of hybrid supercapacitor.

capacitive performance after incorporating PPy or MnO_2 is clearly indicated by the dramatically enlarged CV encircled area. The capacitances of e-WO_3//PPy and e-WO_3//MnO_2 at a high scan rate (20 mV s^{-1}) can reach 11.38 and 14.21 mF cm^{-2}, respectively, and are ~5 times and 7 times higher than that of pure e-WO_3 based supercapacitors (2.22 mF cm^{-2}) at the same scan rate. The enhancement of the capacitance can be intuitionally confirmed by the galvanostatic curves shown in Fig. 7b (Fig. S4† as well). At the charging/discharging rate of 1 mA cm^{-2}, the capacitance enhancement is more obvious.

As shown in Fig. 7b, the e-WO_3//MnO_2 hybrid supercapacitor possesses a capacitance of 45 mF cm^{-2}, which is much higher than that of the pure e-WO_3 based supercapacitor. Also, this impressive capacitance achieved by hybrid supercapacitors is much larger than that of other electrochromic supercapacitors without the hybrid design, as shown in Table S2.†

Besides these greatly enhanced performances, the smart function is also well maintained. The photos of the electrodes of the hybrid supercapacitors at different EESs are shown in Fig. 7c and d. Evidently, the color changes for the hybrid supercapacitors are visibly identical to that of the pure e-WO_3 based supercapacitors shown in Fig. 4a. In addition, the EES of the capacitor can be accurately and quantifiably obtained from the normalized optical density due to the fixed relationship between them for as-prepared e-WO_3 as described by eqn (2). Based on this, the EES of the hybrid supercapacitors may also be quantitatively determined using simple optical transmission measurements, followed by calculating the optical density at 625 nm.

However, it should be noted that the EES obtained here represents the EES of the whole device. And this EES may not be identical to the EES of the e-WO_3 part (EES_w) due to the hybrid charging/discharging dynamics. But there will be a relationship between the EES and EES_w ($EES_w = f(EES)$). Thus, the relationship between the optical density and the EES can be revised as:

$$\log(T_0/T_{EES}) = \eta \times f(EES) \times Q_w \quad (3)$$

where η, the coloring efficiency, is just related to the nature of the as-prepared e-WO_3, and Q_w will be a constant at a certain charging and discharging rate. Herein, the dependence between the optical densities at 625 nm and EESs of the hybrid supercapacitors might be revealed by a calibration curve. Fig. 7e and f exhibit the optical densities at 625 nm *vs.* the representative EESs (0%, 20%, 40%, 60%, 80% and 100%) for the electrodes of e-WO_3//PPy and e-WO_3//MnO_2, respectively. The e-WO_3//PPy hybrid supercapacitor exhibits a convex calibration curve while the e-WO_3//MnO_2 hybrid supercapacitor shows a concave calibration curve, as shown in Fig. 7e and f, respectively. The shape of the calibration curves includes information about the hybrid charging/discharging processes. As long as the calibration curves are generated, the EESs of any types of hybrid supercapacitor can be quantitatively determined by simple optical transmission measurement. For example, an optical density of 0.11 and 0.31 at 625 nm represents an EES of 30% and 90%, respectively, for the e-WO_3//PPy hybrid supercapacitors. Based on the analysis from before, the EES of the hybrid supercapacitors can be visually indicated by the color change of e-WO_3 and quantifiably determined by the calibration curves, which means e-WO_3 can be integrated with other active materials to form a smart hybrid supercapacitor.

4. Conclusions

In conclusion, three advances in smart supercapacitors were achieved in this paper. (1) A visualized indicator was developed for supercapacitor devices by using e-WO_3 as an active material. The color change of the electrode can be used to estimate the potential and EES of the supercapacitor. (2) By introducing concepts in electrochromic studies and the detailed investigations of the optical spectra of the supercapacitor, the normalized optical densities were found to linearly depend on the EES of the e-WO_3 based supercapacitor. This finding quantifies the color change of the e-WO_3 electrodes, as well as clarifies that, instead of the potential, the EES can be associated with color change directly. In addition, this finding makes it possible to quantitatively determine the EES of the supercapacitor using a simple optical transmission test. (3) Hybrid supercapacitors with a parallel structure were developed in order to integrate the color-change EES indicator for high performance supercapacitors. Utilizing the developed method, the e-WO_3 electrode based EES indicator can be integrated into any type of supercapacitor to achieve both high capacitive performances and the smart functions. In addition, we established a strategy to produce a calibration curve for each type of hybrid supercapacitor, which enables the precise, quantitative determination of their EESs using simple optical transmission measurements. The approaches developed in this research make it possible to equip color-change based EES indicators for any energy storage device and determine their EES easily using simple optical transmission measurements. Moreover, since the principle of this EES indicator is based on the electrochromic phenomenon of e-WO_3, which can be continuously colored with the charging process, it can also be used as an EES indicator for asymmetric supercapacitors, whose potential window is larger. Thus, the application areas can be wider. These may greatly extend the applications of the electrochromic materials in energy storage devices for smart function integration.

Acknowledgements

This research was partially supported by a grant from the Research Grants Council of the Hong Kong Special Administrative Region, China (Project No. CityU 109213), and the Science Technology and Innovation Committee of Shenzhen Municipality (the Grant No. JCYJ20140419115507579).

Notes and references

1 J. Miller and P. Simon, *Science*, 2008, **321**, 651–652.
2 P. Simon and Y. Gogotsi, *Nat. Mater.*, 2008, **7**, 845–854.
3 H. Guan, X. Wang, H. Li, C. Zhi, T. Zhai, Y. Bando and D. Golberg, *Chem. Commun.*, 2012, **48**, 4878–4880.

4 X. Wang, W. Tian, D. Liu, C. Zhi, Y. Bando and D. Golberg, *Nano Energy*, 2013, **2**, 257–267.
5 N. Kumar, H. Choi, Y. Shin, D. Chang, L. Dai and J. Baek, *ACS Nano*, 2012, **6**, 1715–1723.
6 T. Chen and L. Dai, *Mater. Today*, 2013, **16**, 272–280.
7 W. Meng, W. Chen, L. Zhao, Y. Huang, M. Zhu, Y. Huang, Y. Fu, F. Geng, J. Yu, X. Chen and C. Zhi, *Nano Energy*, 2014, **8**, 133–140.
8 Q. Weng, X. Wang, X. Wang, C. Zhang, X. Jiang, Y. Bando and D. Golberg, *J. Mater. Chem. A*, 2015, **3**, 3097–3102.
9 D. Liu, X. Wang, X. Wang, W. Tian, J. Liu, C. Zhi, D. He, Y. Bando and D. Golberg, *J. Mater. Chem. A*, 2013, **1**, 1952–1955.
10 X. Wang, Y. Zhang, C. Zhi, X. Wang, D. Tang, Y. Xu, Q. Weng, X. Jiang, M. Mitome, D. Golberg and Y. Bando, *Nat. Commun.*, 2013, **4**, 2905.
11 Y. Qian, R. Liu, Q. Wang, J. Xu, D. Chen and G. Shen, *J. Mater. Chem. A*, 2014, **2**, 10917–10922.
12 W. Tian, X. Wang, C. Zhi, T. Zhai, D. Liu, C. Zhang, D. Golberg and Y. Bando, *Nano Energy*, 2013, **2**, 754–763.
13 Z. Ma, X. Huang, S. Dou, J. Wu and S. Wang, *J. Phys. Chem. C*, 2014, **118**, 17231–17239.
14 X. Lu, T. Zhai, X. Zhang, Y. Shen, L. Yuan, B. Hu, L. Gong, J. Chen, Y. Gao, J. Zhou, Y. Tong and Z. Wang, *Adv. Mater.*, 2012, **24**, 938–944.
15 L. Gao, X. Wang, Z. Xie, W. Song, L. Wang, X. Wu, F. Qu, D. Chen and G. Shen, *J. Mater. Chem. A*, 2013, **1**, 7167–7173.
16 N. Liu, W. Ma, J. Tao, X. Zhang, J. Su, L. Li, C. Yang, Y. Gao, D. Golberg and Y. Bando, *Adv. Mater.*, 2013, **25**, 4925–4931.
17 T. Chen, Y. Xue, A. Roy and L. Dai, *ACS Nano*, 2013, **8**, 1039–1046.
18 J. Bae, M. Song, Y. Park, J. Kim, M. Liu and Z. Wang, *Angew. Chem., Int. Ed.*, 2011, **50**, 1683–1687.
19 L. Yuan, X. Lu, X. Xiao, T. Zhai, J. Dai, F. Zhang, B. Hu, X. Wang, L. Gong, J. Chen, C. Hu, Y. Tong, J. Zhou and Z. Wang, *ACS Nano*, 2012, **6**, 656–661.
20 D. Yu, K. Goh, H. Wang, L. Wei, W. Jiang, Q. Zhang, L. Dai and Y. Chen, *Nat. Nanotechnol.*, 2014, **9**, 555–562.
21 L. Yuan, B. Yao, B. Hu, K. Huo, W. Chen and J. Zhou, *Energy Environ. Sci.*, 2013, **6**, 470–476.
22 Y. Huang, M. Zhu, W. Meng, Y. Fu, Z. Wang, Y. Huang, Z. Pei and C. Zhi, *RSC Adv.*, 2015, **43**, 33981–33989.
23 S. Wang, B. Pei, X. Zhao and R. Dryfe, *Nano Energy*, 2013, **2**, 530–536.
24 J. Xu, H. Wu, L. Lu, S. Leung, D. Chen, X. Chen, Z. Fan, G. Shen and D. Li, *Adv. Funct. Mater.*, 2014, **24**, 1840–1846.
25 X. Wang, B. Liu, R. Liu, Q. Wang, X. Hou, D. Chen, R. Wang and G. Shen, *Angew. Chem., Int. Ed.*, 2014, **53**, 1849–1853.
26 P. Yang, X. Xiao, Y. Li, Y. Ding, P. Qiang, X. Tan, W. Mai, Z. Lin, W. Wu, T. Li, H. Jin, P. Liu, J. Zhou, C. Wong and Z. Wang, *ACS Nano*, 2013, **7**, 2617–2626.
27 X. Chen, H. Lin, J. Deng, Y. Zhang, X. Sun, P. Chen, X. Fang, Z. Zhang, G. Guan and H. Peng, *Adv. Mater.*, 2014, **26**, 8126–8132.
28 P. Yang, P. Sun, Z. Chai, L. Huang, X. Cai, S. Tan, J. Song and W. Mai, *Angew. Chem., Int. Ed.*, 2014, **126**, 12129–12133.
29 Y. Tian, S. Cong, W. Su, H. Chen, Q. Li, F. Geng and Z. Zhao, *Nano Lett.*, 2014, **14**, 2150–2156.
30 B. Reddy, P. Kumar and M. Deepa, *ChemPhysChem*, 2015, **16**, 377–389.
31 Z. Xie, X. Jin, G. Chen, J. Xu, D. Chen and G. Shen, *Chem. Commun.*, 2013, **50**, 608–610.
32 H. Wei, X. Yan, S. Wu, Z. Luo, S. Wei and Z. Guo, *J. Phys. Chem. C*, 2012, **116**, 25052–25064.
33 G. Cai, X. Wang, M. Cui, P. Darmawan, J. Wang, A. Eh and P. Lee, *Nano Energy*, 2015, **12**, 258–267.
34 M. Zhu, W. Meng, Y. Huang, Y. Huang and C. Zhi, *ACS Appl. Mater. Interfaces*, 2014, **6**, 18901–18910.
35 D. DeLongchamp and P. T. Hammond, *Adv. Mater.*, 2001, **13**, 1455–1459.
36 B. P. Jelle and G. Hagen, *Sol. Energy Mater. Sol. Cells*, 1999, **58**, 277–286.
37 J. Tao, N. Liu, W. Ma, L. Ding, L. Li, J. Su and Y. Gao, *Sci. Rep.*, 2013, **3**, 2286.
38 J. Tao, N. Liu, L. Li, J. Su and Y. Gao, *Nanoscale*, 2014, **6**, 2922–2928.
39 Y. Huang, J. Tao, W. Meng, M. Zhu, Y. Huang, Y. Fu, Y. Gao and C. Zhi, *Nano Energy*, 2015, **11**, 518–525.
40 Y. Huang, Y. Huang, W. Meng, M. Zhu, H. Xue, C. Lee and C. Zhi, *ACS Appl. Mater. Interfaces*, 2015, **7**, 2569–2574.
41 Y. Gogotsi and P. Simon, *Science*, 2011, **334**, 917–918.
42 J. Wang, E. Khoo, P. S. Lee and J. Ma, *J. Phys. Chem. C*, 2008, **112**, 14306–14312.
43 O. Schirmer, V. Wittwer, G. Baur and G. Brandt, *J. Electrochem. Soc.*, 1977, **5**, 749–753.
44 E. Ozkan, S. Lee, C. Tracy, J. Pitts and S. Deb, *Sol. Energy Mater. Sol. Cells*, 2003, **4**, 439–448.
45 J. Zhang, D. Benson, C. Tracy, S. Deb, A. Czanderna and C. Bechinger, *J. Electrochem. Soc.*, 1997, **6**, 2022–2026.
46 C. Li, J. H. Hsieh, M. Hung and B. Q. Huang, *Thin Solid Films*, 2015, **587**, 75–82.
47 S. Lee, R. Deshpande, P. Parilla, K. Jones, B. To, A. Mahan and A. Dillon, *Adv. Mater.*, 2006, **6**, 763–766.